







Multimodal approach to explore the pathogenicity of BARD1, ARG 658 CYS, and ILE 738 VAL mutants

Rajan Kumar Choudhary, Vikrant, Quadir M. Siddiqui, Pankaj S. Thapa, Sweta Raikundalia, Nikhil Gadewal, Nachimuthu Senthil Kumar, M.V. Hosur & Ashok K. Varma

To cite this article: Rajan Kumar Choudhary, Vikrant, Quadir M. Siddiqui, Pankaj S. Thapa, Sweta Raikundalia, Nikhil Gadewal, Nachimuthu Senthil Kumar, M.V. Hosur & Ashok K. Varma (2016) Multimodal approach to explore the pathogenicity of BARD1, ARG 658 CYS, and ILE 738 VAL mutants, Journal of Biomolecular Structure and Dynamics, 34:7, 1533-1544, DOI: [10.1080/07391102.2015.1082149](https://doi.org/10.1080/07391102.2015.1082149)

To link to this article: <https://doi.org/10.1080/07391102.2015.1082149>

 View supplementary material  Accepted author version posted online: 26 Aug 2015.
Published online: 23 Sep 2015. Submit your article to this journal  Article views: 153 View related articles  View Crossmark data  Citing articles: 2 View citing articles 

Multimodal approach to explore the pathogenicity of BARD1, ARG 658 CYS, and ILE 738 VAL mutants

Rajan Kumar Choudhary^a, Vikrant^{a,†}, Quadir M. Siddiqui^a, Pankaj S. Thapa^a, Sweta Raikundalia^a, Nikhil Gadewal^a, Nachimuthu Senthil Kumar^b, M.V. Hosur^a and Ashok K. Varma^{a*}

^aAdvanced Centre for Treatment, Research and Education in Cancer, Kharghar, Navi Mumbai 410 210, Maharashtra, India;

^bDepartment of Biotechnology, Mizoram University (A Central University), Aizawl 796 004, Mizoram, India

Communicated by Ramaswamy H. Sarma

(Received 28 May 2015; accepted 7 August 2015)

BARD1–BRCA1 complex plays an important role in DNA damage repair, apoptosis, chromatin remodeling, and other important processes required for cell survival. BRCA1 and BARD1 heterodimer possess E3 ligase activity and is involved in genome maintenance, by functioning in surveillance for DNA damage, thereby regulating multiple pathways including tumor suppression. BRCT domains are evolutionary conserved domains present in different proteins such as BRCA1, BARD1, XRCC, and MDC1 regulating damage response and cell-cycle control through protein–protein interactions. Nonetheless, the role of BARD1BRCT in the recruitment of DNA repair mechanism and structural integrity with BRCA1 complex is still implicit. To explicate the role of BARD1BRCT in the DNA repair mechanism, *in silico*, *in vitro*, and biophysical approach were applied to characterize BARD1 BRCT *wild-type* and Arg658Cys and Ile738Val mutants. However, no drastic secondary and tertiary structural changes in the mutant proteins were observed. Thermal and chemical denaturation studies revealed that mutants Arg658Cys and Ile738Val have a decrease in T_m and ΔG than the *wild type*. *In silico* studies of BARD1 BRCT (568–777) and mutant protein indicate loss in structural compactness on the Ile738Val mutant. Comparative studies of *wild-type* and mutants will thus be helpful in understanding the basic role of BARD1BRCT in DNA damage repair.

Keywords: BARD1 BRCT; protein–protein interactions; secondary and tertiary structure; thermal and chemical denaturation

1. Introduction

Breast cancer is one of the prominent causes for cancer deaths in the developing countries. It has been found that mutations in the *BRCA1* and *BRCA2* genes can predispose someone at the risk of developing breast and ovarian cancer (Collins et al., 1995; Miki et al., 1994; Wooster et al., 1994). The inherited germ line mutations in the genes like *RAD50*, *ATM*, *CHEK2*, *NBS1*, *53BP1*, *PALB2*, *BRIP1* *BRCA 1/2*, and *BARD1* regulate genomic integrity and cancer predisposing factors (Ahmed & Rahman, 2006; Heikkinen et al., 2006; Karppinen et al., 2006; Meijers-Heijboer et al., 2002; Rapakko, Heikkinen, Karppinen, Erkkö, & Winqvist, 2007; Renwick et al., 2006). BARD1 is a structurally correlated but sequentially distinct protein from BRCA1. BARD1 and BRCA1 both harbor N-terminal RING domain and two C-terminal tandem BRCT repeat motifs (Wu et al., 1996). BARD1 contains four ankyrin repeats in the region (425–550), which is absent in BRCA1. BRCA1 and BARD1 heterodimerize by RING–RING domain interaction and colocalize to distinct nuclear assemblies at different stages

of cell-cycle progression (Jin et al., 1997; Scully et al., 1997). Furthermore, *in vivo* BRCA1–BARD1 heterodimer forms active E3 ubiquitin ligase complex, and plays a significant role in tumor suppression (Brzovic, Meza, King, & Klevit, 2001; Brzovic, Rajagopal, Hoyt, King, & Klevit, 2001; Wu-Baer, Lagazon, Yuan, & Baer, 2003). Mis-sense mutations within the BRCA1 RING domain lead to loss in heterodimerization which further reduces E3 ubiquitin ligase activity (Brzovic, Meza, et al., 2001). BARD1 BRCT (568–777) domain is conserved in many other multiple DNA damage response (DDR) proteins (Bork et al., 1997; Callebaut & Mornon, 1997).

Different DDR proteins have diverse repeats of BRCTs (Mohammad & Yaffe, 2009). It has been reported that BARD1 BRCT is required for the early recruitment of BRCA1 at the DNA damage site (Li & Yu, 2013). Noting the role of BARD1 in genomic integrity, we decided to explore functional consequences of genetic alterations discovered in the BARD1 BRCT region. Two cancer predisposing mutations, Arg658Cys in Caucasian, African, Finnish populations, and Ile738Val in Polish and

*Corresponding author. Email: avarma@actrec.gov.in

[†]Current address: Quintiles Research Pvt. Ltd. Andheri, Mumbai-400059, India.

Belgian families have been detected (Alshatwi, Hasan, Syed, Shafi, & Grace, 2012; Antoniou et al., 2010; De Brakeleer et al., 2010; Karppinen, Heikkinen, Rapakko, & Winqvist, 2004; Thai et al., 1998), but the molecular mechanism of how these mutations of BARD1 gene lead to breast cancer has not been explored. Further, in sporadic and BRCA1-associated breast cancers, expression of BARD1 is observed to be too low suggesting a significant role of BARD1 in breast carcinogenesis (Ghimenti et al., 2002; Yoshikawa et al., 2000).

In this study, we have used *in vitro* experiments and *in silico* approaches to understand the folding pattern of BARD1 BRCT (568-777) and its two cancer-disposing mutants, Arg658Cys and Ile738Val. Molecular dynamics simulations (MDS) were carried out to explore alterations in the structure at the atomic level. To our conclusion, both the mutants show loss in thermodynamic stability; however, BARD1 Ile738Val protein structure shows higher structural flexibility.

2. Material and methods

2.1. Molecular dynamics simulation

The crystal structure of BARD1 BRCT (568-777) *wild-type* protein was taken from PDB (pdb id: 2NTE), (Birrane, Varma, Soni, & Ladas, 2007). BARD1 BRCT (568-777) amino acid sequence was retrieved from the Uniprot database (Accession ID: q99728). Point mutants, Arg658Cys and Ile738Val, were introduced using SPDB viewer (Kaplan & Littlejohn, 2001). MDS was performed using GROMACS 4.5.5 package (Hess, Kutzner, van der Spoel, & Lindahl, 2008) installed on a 80-node cluster of Xeon quad-core processors. The molecular systems were solvated with TIP3P water molecules in a cubic box with periodic boundary conditions of 1.0 nm from the edge of the box. Counter ions were added to neutralize the systems. The systems were subjected to energy minimization for 5000 iterations by steepest descent algorithm implementing under OPLS-AA force field (Kaminski, Friesner, Tirado-Rives, & Jorgensen, 2001) with a tolerance of 1000 kJ/mol/nm. Electrostatic, columbic, and van der Waals interactions were calculated with a distance cut-off of 1.4 nm. Systems were equilibrated using NVT (Moles Volume Temperature) followed by NPT (Moles Pressure Temperature) ensemble for 50,000 steps each. SHAKE algorithm (Ryckaert, Ciccotti, & Berendsen, 1977) was used to constrain bond lengths. Finally, systems were subjected to MD simulation for 50 ns of production run with time-step integration of 2 fs. The trajectories were saved at every 2 ps and analyzed using GROMACS. The comparative analysis of BARD1 BRCT (568-777) *wild-type* and mutant structures, Arg658Cys, Ile738Val, were performed to calculate the RMSD, RMSF, radius of gyration, solvent

accessible surface area (SASA), Dictionary of secondary structure pattern (DSSP) (Kabsch & Sander, 1983), and hydrogen-bond interactions.

2.2. Principal component analysis

Principal component (PC) was calculated using eigenvectors and eigenvalues for the covariance matrix. Projection of first two principal components was carried out by essential dynamics method described within the GROMACS package (Amadei, Linssen, & Berendsen, 1993). After removing the rotational and translational movements, variance/covariance matrix was built and further eigenvectors and eigenvalues were calculated. The eigenvalues are representative of amplitude of eigenvectors in multidimensional space. The concerted motion of the protein can be detected by the displacement of atoms along each eigenvector.

2.3. Protein expression and purification

BARD1 BRCT (568-777) *wild-type* protein was cloned in pET-28a vector (cDNA of full-length BARD1 was kind gift from Prof. Richard Bayer, Institute of Cancer Genetics, Columbia University). Mismatch primer method of site-directed mutagenesis was used to generate the Arg658Cys and Ile738Val mutants (forward primer Arg 658Cys 5'-GAAATTCCTGAAGGTCCATGCAGAAAGC-AGGCTCAACAG-3', reverse primer 5'-CTGTTGAGCC-TGCTTCTGCATGGACCTTCAGGAATTTC-3', forward primer Ile738Val 5'-CTGCACACAGTATATCGTCTAT-GAAGATTTGTGT-3' reverse primer 5'-ACACAAATC-TTCATAGACGATATACTGTGTGCAG-3'). The BARD1 BRCT (568-777) *wild-type*, Arg658Cys, and Ile738V mutant proteins were expressed and purified in 6His fusion proteins using Rosetta 2(DE3) bacterial cells. Fusion proteins were first purified on Ni-NTA affinity chromatography, then further treated with TEV to remove the fusion tag. Protein was purified using AKTA FPLC size exclusion chromatography on superdex 75 column (GE Healthcare).

2.4. Dynamic light scattering experiment

Purified BARD1 BRCT (568-777), Arg658Cys, and Ile738Val mutant proteins were analyzed on Malvern particle size analyzer (Zetasizer μ V) dynamic light scattering instrument to characterize the oligomeric nature of these proteins. The protein samples were filtered (0.22- μ m filter) and degassed prior to scanning. 1.0 mg/ml of *wild-type* and mutant proteins were scanned at 5-min intervals for 15 min, and effective diameters were obtained from peak positions. The experiments were repeated three times and the average was considered to be the true value.

2.5. Circular dichroism spectroscopy

Circular dichroism spectroscopy was performed using different concentrations of purified proteins on the JASCO-815 spectropolarimeter. For far-UV CD spectra, the protein concentration was 10 μ M and the wavelength range was taken from $\lambda = 200$ –240 nm, and for near-UV spectra, the wavelength range was from $\lambda = 350$ –250 nm with the protein concentration of 40 μ M (buffer: 2.5 mM HEPES pH 7.5, 50 mM NaCl). Blank-corrected seven independent data scans were averaged, and the average value is presented for further comparative structural analysis. Furthermore, proteins at a concentration of 10 μ M were unfolded in a temperature range from 10 to 65°C, and folding pattern was monitored by measuring ellipticity at $\lambda = 222$ nm. Near-UV range, thermal denaturation studies were performed for 40 μ M of proteins at different temperatures 20, 30, 45, and 60°C. The observed values of fractions unfolded were used for curve fitting.

2.6. Limited proteolysis

BARD1 BRCT *wild-type* and mutant proteins (2 mg/ml) were treated with trypsin (37°C) and chymotrypsin (25°C), 10 μ g/ μ l each in the digestion cocktail. At the time points of 0, 5, 10, 30, 60, 120, and 180 min, the reaction was stopped by adding protease inhibitor PMSF (1 mM). The experiment was repeated thrice considering untreated *wild-type* and mutant samples as controls.

2.7. Fluorescence spectroscopy

2.7.1. Chemical denaturation

Micro-environment of tryptophan residue in the proteins were investigated using fluorescence spectrophotometer (Horiba, USA). While the excitation was at $\lambda = 295$ nm, the individual fluorescence emission spectra were recorded from $\lambda = 310$ –400 nm. In chemical denaturation, BARD1 BRCT proteins (2 μ M) were treated with increasing concentrations of GuHCl (0–6 M) keeping the final volume constant, and emission spectra were recorded between $\lambda = 310$ and 400 nm. Averaged blank-corrected data were analyzed by fitting to a three-state transition model (Pace, 1986; Pace & Shaw, 2000; Vikrant et al., 2013).

2.7.2. Data analysis and curve fitting

Thermodynamic parameters were determined during the GuHCl unfolding process by detecting the folded (*N*) to intermediate (*I*) and intermediate to unfolded (*U*) transitions of the curve. Further, thermodynamic constraints analysis and curve fitting were performed (Pace & Shaw, 2000; Vikrant, Nakhwa, Badgujar, Kumar, & Rathore, 2014).

2.8. Chemical cross-linking assay

BARD1 BRCT (568–777) *wild-type* and mutant proteins were incubated with 0.1% glutaraldehyde, and the reaction was terminated by addition of 5 μ l of 1 M Tris pH-8.0. Reaction was stopped in a time-dependent manner (0, 2.5, 5, 10, 15, 30, and 60 min, respectively) and analyzed on 12% SDS-PAGE. Untreated protein sample was taken as control.

3. Results and discussion

Deleterious non-synonymous single nucleotide polymorphisms (nsSNPs) are involved in inducing disease-associated phenomena, because of structural alterations and consequent loss of molecular functions. The modern bioinformatics-based advanced methods have now enabled us to determine the structural effects due to deleterious nsSNPs in the target candidate genes. In the current study, multidisciplinary, *in vitro*, biophysical, and *in silico* approaches were employed to understand the pathogenicity of BARD1 BRCT, Arg658Cys, and Ile738Val mutants (Figure 1(F)).

3.1. Folding pattern of BARD1 BRCT (568–777) *wild-type* and mutants

BARD1 BRCT, Arg658Cys, and Ile738Val mutations have been discovered from the affected families of breast and ovarian cancer. Considering the importance of mutations in predisposing the cancer risk, we decided to characterized abrogative effect of mutations on the structure and function of the protein. It has been well documented that different classes of proteins with exposed hydrophobic residues become highly prone to non-specific interactions (Kolchanov, Soloviov, & Zharkikh, 1983; Zhukov, Jaroszewski, & Bierzynski, 2000), which in turn lead to the formation of high molecular weight aggregates. The residual Arg658Cys mutation is the substitution of a basic amino acid to a small non-polar residue, cysteine. However, Ile738Val substitution is a change from a large to small hydrophobic residue. Ile to Val mutation leads to removal of $-\text{CH}_2$ -group from Ile, and potentially create a void volume of 25 \AA^3 in the mutant protein (Harpaz, Gerstein, & Chothia, 1994). Such mutations may lead to the loss of hydrophobic interactions and van der Waals interactions among the substituted and neighboring residues. To explore this prospect, we have used gel filtration chromatography (AKTA FPLC, superdex 75 column) to probe the oligomeric status of the mutants Arg658Cys and Ile738Val. The non-synonymous amino acid substitution in protein tends to show differential solubility and elution profiles in gel filtration chromatography. There was no substantial alteration in solubility and elution profiles of Arg658Cys and

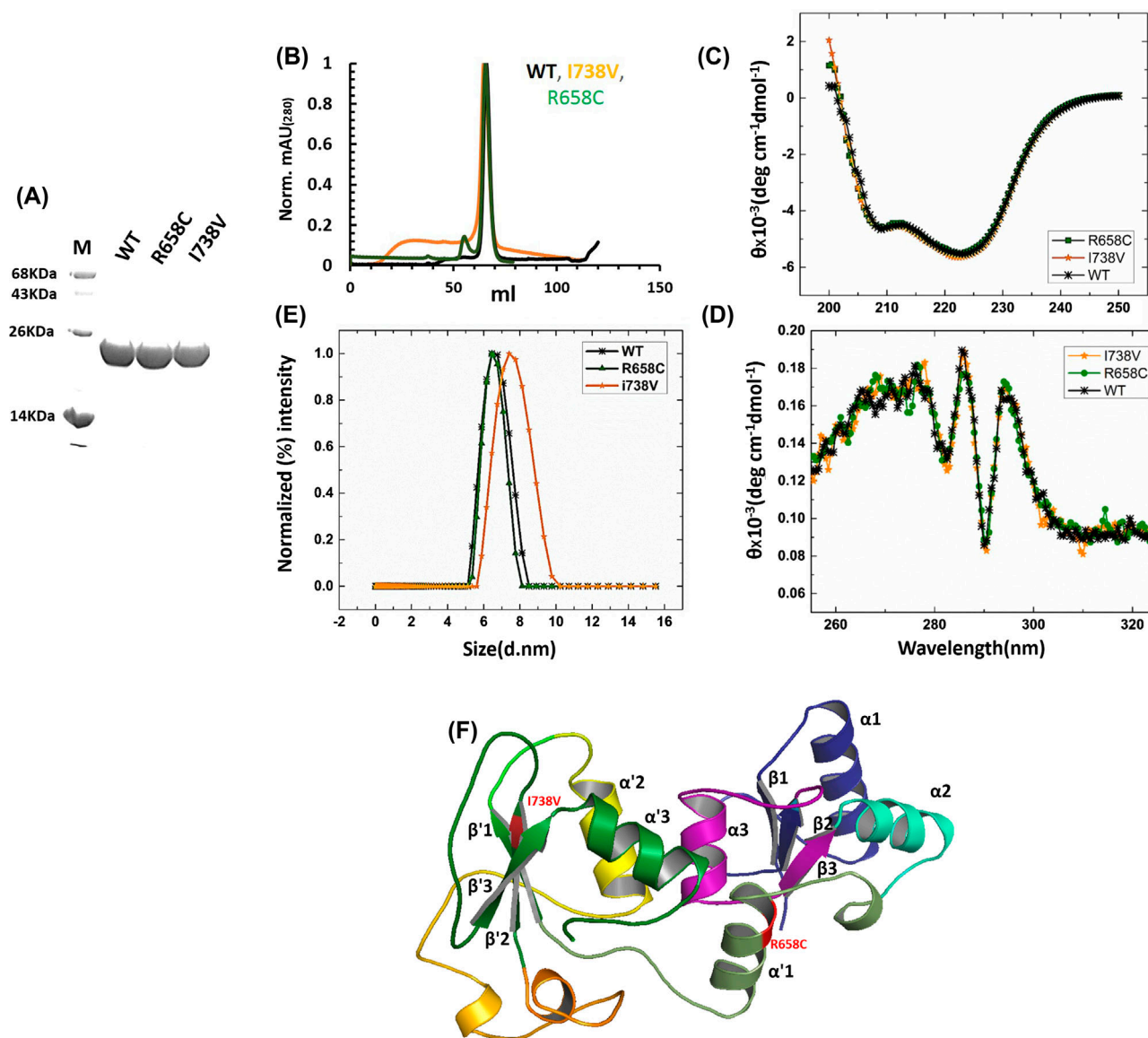


Figure 1. Expression and purification profile of BARD1 BRCT (568-777) *wild-type*, Arg658Cys, and Ile738Val proteins. Notes: (A) Purified protein after gel filtration chromatography on SDS-PAGE. FPLC purified protein were heated with Laemmli buffer and loaded on SDS-PAGE BARD1 BRCT (568-777) *wild-type* (lane 1), Arg658Cys (lane 2), and Ile738Val (lane 3). (B) Comparative gel filtration spectra of BARD1 BRCT (568-777) *wild-type*, Arg658Cys, and Ile738Val (Superdex-75, GE). Elution profile of BARD1 BRCT (568-777) *wild-type*, Arg658Cys, and Ile738Val were similar and showed the presence of single peak corresponding to monomer. (C) BARD1 BRCT (568-777), Arg658Cys, and Ile738Val have well-defined α/β characteristics and mutants does not show any drastic alteration in the secondary structure. (D) Overlay of near-UV spectra of BARD1 BRCT (568-777) *wild-type*, Arg658Cys, and Ile738Val mutant proteins indicating well compact overall structure. (E) Dynamic light scattering profile of BARD1 BRCT (568-777) *wild-type*, Arg658Cys, and Ile738Val showed monomeric population of all the proteins. (F) Crystal structure of BARD1 BRCT (PDB ID: 2NTE) with the sites for cancer-predisposing mutations. Mutant residues are indicated in red.

Ile738Val mutant. In size exclusion chromatography, *wild-type* as well as mutants elute at the same position in superdex 75 column (GE) (Figure 1(A) and (B)). Hence, it is concluded that Arg658Cys and Ile 738Val mutations are not affecting the monomeric nature of BARD1 BRCT (568-777) *wild-type* protein in solution. This monomeric behavior of BARD1 BRCT (568-777) *wild-type*,

Arg658Cys, and Ile 738Val mutant proteins were further supported by chemical cross-linking experiments (Supplementary Figure 1A). No higher molecular aggregate formations were observed using cross-linking assay of BARD1 BRCT (568-777) *wild-type*, Arg658Cys, and Ile738Val proteins. Furthermore, dynamic light scattering of BARD1 BRCT (568-777) *wild-type*, Arg658Cys, and

Ile738Val mutant samples also indicated their monomeric nature. Albeit, BARD1 BRCT (568-777) *wild-type* and Arg658Cys did not show any change in hydrodynamic size, a slight increment was observed in Ile738Val mutant protein (Figure 1(E)). The hydrodynamic diameter of BARD1 BRCT (568-777) *wild-type* and Arg658Cys proteins were found to be 6.44 ± 0.45 nm, whereas Ile738Val mutant protein showed a diameter of $7.40 \pm .23$ nm. The relative increase in effective hydrodynamic size indicates molecular expansion in Ile738Val mutant. Relative increase in the hydrodynamic radii in Ile738Val mutant may be due to the void volume generated in the hydrophobic core of the protein. This may further increase the conformational entropy of neighboring residues making mutant protein structurally more flexible and leading to the increase in effective hydrodynamic diameter of the protein.

3.2. Structural organization

Far-UV CD spectra show predominant α -helix and β -strand characteristic, and no significant differences were observed in the mean residual ellipticities of *wild-type* and mutant proteins (Figure 1(C)). Near-UV CD spectra were obtained to dissect the effect of mutations on overall packing of the protein. Comparative near-UV spectra of BARD1 BRCT (568-777) *wild-type*, Arg658Cys, and Ile738Val mutant proteins do not reveal

change in ellipticity, hence mutations are not abrogating the tertiary structure of BARD1 BRCT (568-777) *wild-type* protein (Figure 1(D)). Treating with trypsin (10 μ g/mol) and chymotrypsin (10 μ g/mol) for three hours, the pattern on 12% SDS-PAGE for the *wild-type* and both the mutant proteins was very similar (Figure 2). This observation suggests that the mutants also have compact tertiary structure similar to that of the *wild-type* protein. However, *wild-type* and mutants were different when treated with the chemical denaturant GuHCl. To determine the unfolding pattern of BARD1 BRCT (568-777) *wild-type*, Arg658Cys, and Ile738Val mutant proteins, all proteins with 2 μ M concentration were incubated with increasing concentrations of GuHCl (0–6 M) for 24 h until equilibrium was achieved. Emission maxima were recorded between $\lambda = 310$ and 390 nm. In the absence of GuHCl, while *wild-type* protein shows emission maximum at $\lambda = 333$ nm, the emission maxima for BARD1 BRCT (568-777), Arg658Cys, and Ile738Val mutant proteins were at $\lambda = 336$ and 337 nm, respectively. This red shifting in the emission maximum for the mutants is due to the local change in the environment, resulting in exposure of buried tryptophan to polar solvent interface. BARD1 BRCT *wild-type* and mutant proteins denatured completely in 6 M GuHCl with an emission maximum of $\lambda = 345$ nm, which indicates that tryptophans are exposed to polar interface (Figure 3(A)). Thus, collective observations from CD spectroscopy,

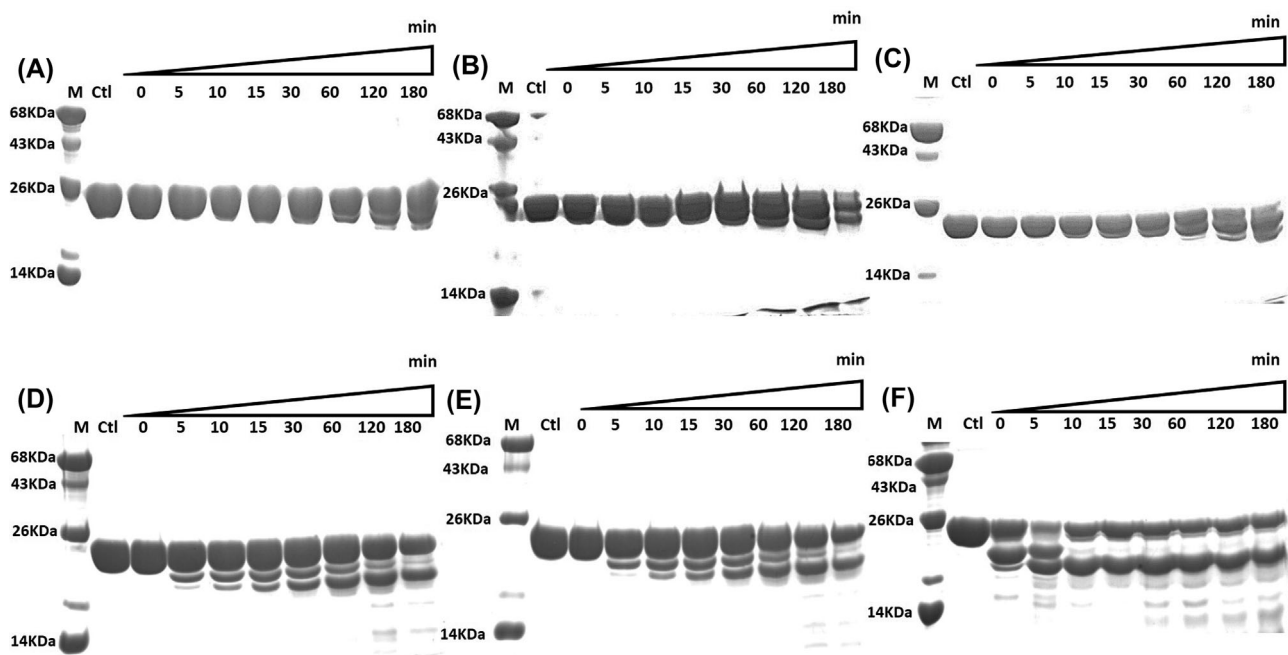


Figure 2. Resistivity profile of BARD1 BRCT (568-777) *wild-type*, Arg658Cys, and Ile738Val toward protease digestion.

Notes: (A) Limited proteolysis of BARD1 BRCT (568-777) *wild-type*, (B) Arg658Cys, and (C) Ile738Val using trypsin and (D) BARD1 BRCT (568-777) *wild-type*, (E) Arg658Cys, and (F) Ile738Val using chymotrypsin as proteases.

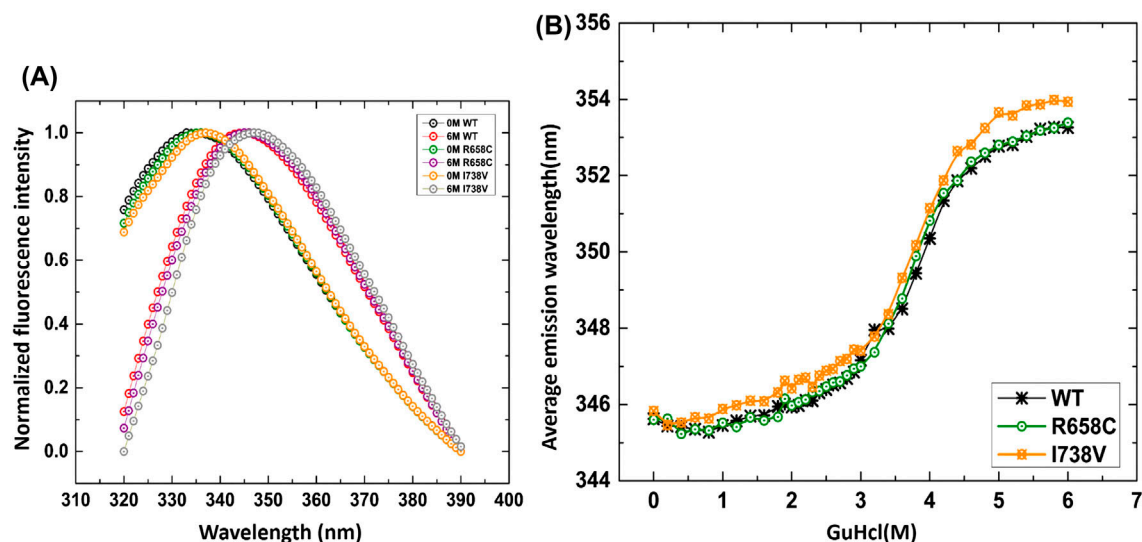


Figure 3. Chemical denaturation profile of BARD1 BRCT (568-777) *wild-type*, Arg658Cys, and Ile738Val.

Notes: (A) Overlay of normalized fluorescent intensity pattern of BARD1 BRCT (568-777) *wild-type*, Arg658Cys, and Ile738Val mutants. Normalized fluorescence intensity of BARD1 BRCT (568-777) *wild-type* native, Arg658Cys, and Ile738Val (0 M GuHCl) unfolded (6 M GuHCl), respectively. (B) Non-linear least-squares fit of a three-state equilibrium unfolding model of BARD1 BRCT (568-777) *wild-type*, Arg658Cys, and Ile738Val on the GuHCl-induced denaturation plot measured at 10°C.

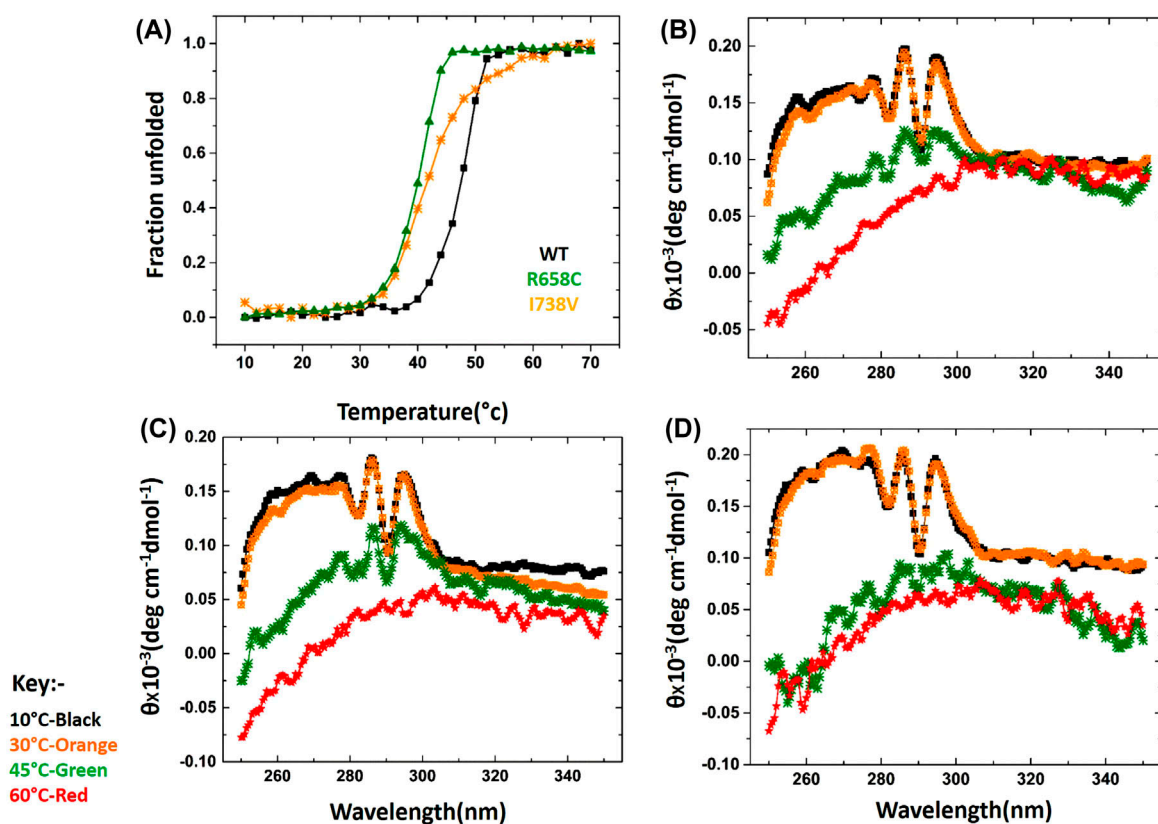


Figure 4. Structure and stability analysis of BARD1 BRCT (568-777) *wild-type*, Arg658Cys, and Ile738Val mutant proteins.

Notes: (A) Overlay of fraction unfolded in far-UV CD spectra of BARD1 BRCT (568-777) *wild-type*, Arg658Cys, and Ile738Val. Thermal stability assessment of BARD1 BRCT (568-777) *wild-type*, Arg658Cys, and Ile738Val in near-UV range. (B) Overlay of mean residual ellipticity obtained after thermal denaturation of BARD1 BRCT (568-777) *wild-type*, (D) Arg658Cys, and (C) Ile738Val in CD spectroscopy.

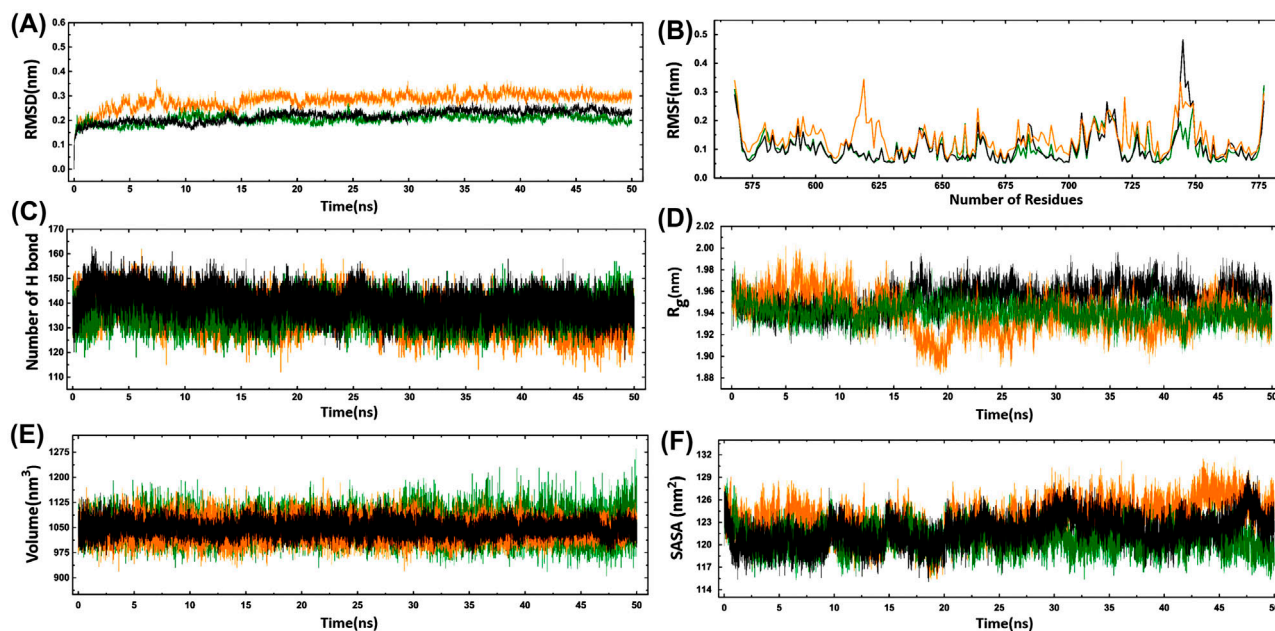


Figure 5. Structural analysis of BARD1 BRCT (568-777) *wild-type* and mutant proteins using molecular dynamics simulation. Notes: Comparative overlay of (A) RMSD, (B) RMSF, (C) N–H bond, (D) R_g , (E) SASA, and (F) volume overlay of BARD1 BRCT (568-777) *wild-type* (black), Arg658Cys (green), and Ile738Val (orange) with respect to time (ns).

limited proteolysis, and fluorescence spectroscopy suggested that Arg658Cys and Ile738Val substitutions might be affecting secondary and tertiary structures only locally, and the effect of mutation is collectively responsible for tertiary structural alterations.

3.3. Thermodynamic stability of BARD1 BRCT (568-777) *wild-type* and mutants

To evaluate unfolding phenomenon and thermodynamic stability, thermal denaturation studies of proteins were performed using CD spectroscopy. The change in ellipticity due to gradual increase in the temperature from 10 to 65°C was recorded. Ellipticity at $\lambda = 222$ nm was used to calculate fractions unfolded (Figure 4(A)). The data obtained from CD at $\lambda = 222$ nm could fit satisfactorily into a two-state denaturation model for *wild-type* and all mutants (Pace, 1986; Pace & Shaw, 2000). The transition mid-point (T_m) calculated for BARD1 BRCT (568-777) *wild-type*, Arg658Cys, and Ile738Val mutant proteins were 40.6, 41.7, and 47.8°C, respectively. The changes in free energies corresponding to the denaturation were: $\Delta G^{\circ} \text{H}_2\text{O}$ 9.6 ± 0.32 , 7.3 ± 0.12 , and $7.6 \pm .42$ kcal/mol, respectively. For tertiary structure stability assessment, near-UV CD spectra of BARD1 BRCT(568-777) *wild-type*, Arg658Cys, and Ile738Val mutant proteins were monitored at four different temperatures: 10, 30, 45, and 60°C corresponding to $\lambda = 280$ and $\lambda = 295$. At the

temperature ranges from 10 to 30°C, BARD1 BRCT (568-777) *wild-type*, Arg658Cys, and Ile738Val, peaks at $\lambda = 295$ nm and $\lambda = 280$ nm were observed, which is characteristic of well folded 3-D structures. Furthermore, at 45°C, BARD1 BRCT (568-777) *wild-type* and Ile738Val mutant proteins show 40% loss in the mean residual ellipticity, but a complete loss in ellipticity was observed in Arg658Cys mutant. It is therefore concluded that BARD1 BRCT (568-777) *wild-type* and Ile738Val mutant proteins have higher thermal stability than Arg658Cys (Figure 4(B)–(D)). Fluorescence spectroscopy was used to monitor unfolding at 283 K induced by GuHCl. For chemical denaturation of BARD1 BRCT (568-777) *wild-type*, Arg658Cys, and Ile738Val mutant proteins, thermodynamic parameters were calculated by plotting average fluorescence emission wavelength against GuHCl concentration (Figure 3(B)). $\Delta G^{\circ} \text{H}_2\text{O}$ for BARD1 BRCT, Arg658Cys, and Ile738Val were $7.19 \pm .36$, $6.29 \pm .41$, and $6.8 \pm .21$ kcal/mol, respectively. This value of the BARD1 BRCT *wild-type* protein is in agreement with the earlier reported results (Thanassoulas et al., 2010). ΔG for folded to intermediate and then from intermediate to unfolded state for *wild-type* proteins was calculated to be 2.68 and 4.5 kcal/mol, for Ile738Val mutant to be 1.8 and 4.8658 kcal/mol, for Arg658Cys mutant to be 2.2 and 4.09 kcal/mol, respectively. Thus, the folded mutants are thermodynamically less stable than the *wild type*.

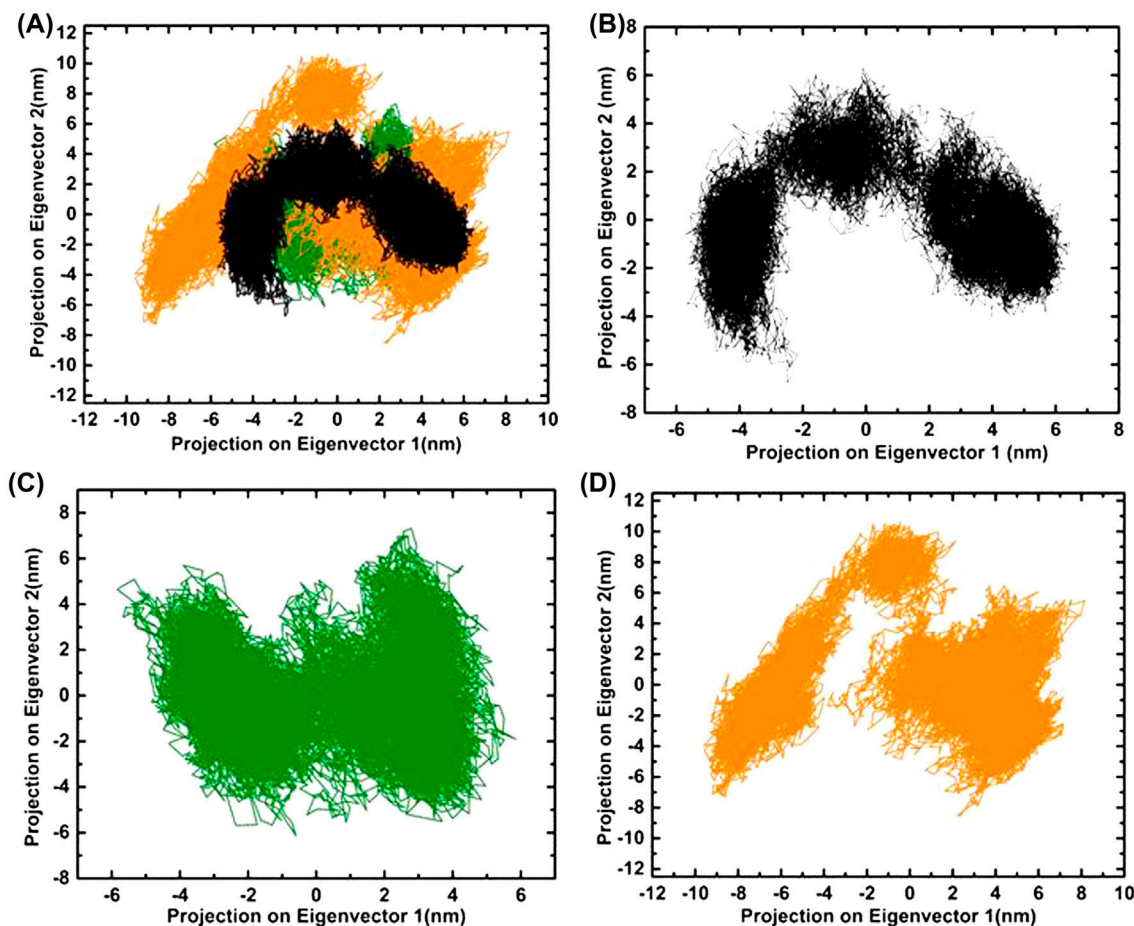


Figure 6. Principal component analysis of BARD1 BRCT (568-777) *wild-type*, Arg658Cys, and Ile738Val proteins. Notes: (A) BARD1 BRCT (568-777) *wild-type*, Arg658Cys, and Ile738Val are shown in black, green, and yellow, respectively. For unblemished perception, individual protein has been represented independently, (B) BARD1 BRCT, (C) Arg658Cys, and (D) Ile738Val. Dynamics of the proteins are projected with two eigenvectors.

3.4. MDS of BARD1 BRCT, ARG658CYS, and ILE 738VAL mutations

Molecular dynamics calculations were performed to visualize the structural alterations in BARD1 BRCT (568-777) *wild-type*, Arg658Cys, and Ile738Val mutant proteins. *Ca*, RMSD values from the input structure were plotted against time (50 ns) (Figure 5(A)). It has been observed that *wild-type* and mutant structures showed similar deviations till 1500 ps, and at 1750 ps, the structures behaved differently. However, after 1.75 ns, Ile738Val mutant structure RMSD increases to about 3 Å, whereas *wild-type* and Ile738Val structures remained with a RMSD value of ~1.75 to 2 Å and ~1.75 to 3 Å, respectively. In BARD1 BRCT (568-777) *wild-type* and Arg658Cys and Ile738Val mutant protein structures, the magnitude of *Ca* RMSD fluctuations, after relaxation period produces stable trajectories throughout the simulation (Figure 5(A)). The RMSF values of BARD1 BRCT (568-777) *wild-type*, Arg658Cys, and Ile738Val mutant

protein structures were obtained, and higher degree of residual flexibility were observed for Ile738Val mutant protein (Figure 5(B)). The BARD1 BRCT (568-777) *wild-type* structure showed radius of gyration (R_g) value of ~1.924 nm at 0 ns, ~1.946 nm at 2 ns, ~1.92 nm at 5 ns, ~1.94 nm at 10 ns, ~1.97 nm at 15 ns, ~1.93 nm at 20 ns, ~1.96 nm at 25 ns, and 1.95 nm at 30 ns. Ile738Val mutant structure showed R_g value of ~1.92 nm at 0 ns, ~1.954 nm at 2 ns, ~1.97 nm at 5 ns, ~1.94 nm at 10 ns, ~1.95 nm at 15 ns, ~1.92 nm at 20 ns, ~1.91 nm at 25 ns, and 1.94 nm at 30 ns. Arg658Cys mutant structure showed R_g value of ~1.925 nm at 0 ns, ~1.94 nm at 2 ns, ~1.95 nm at 5 ns, ~1.94 nm at 10 ns, ~1.95 nm at 15 ns, ~1.93 nm at 20 ns, and ~1.93 nm at 25 ns, and 1.94 nm at 30 ns. Radius of gyration of Arg658Cys mutant protein structure does not show much fluctuation, but Ile738Val mutant protein structure shows great variation throughout 50 ns simulation. Random change in radius of gyration at 20 ns of Ile738Val mutant protein

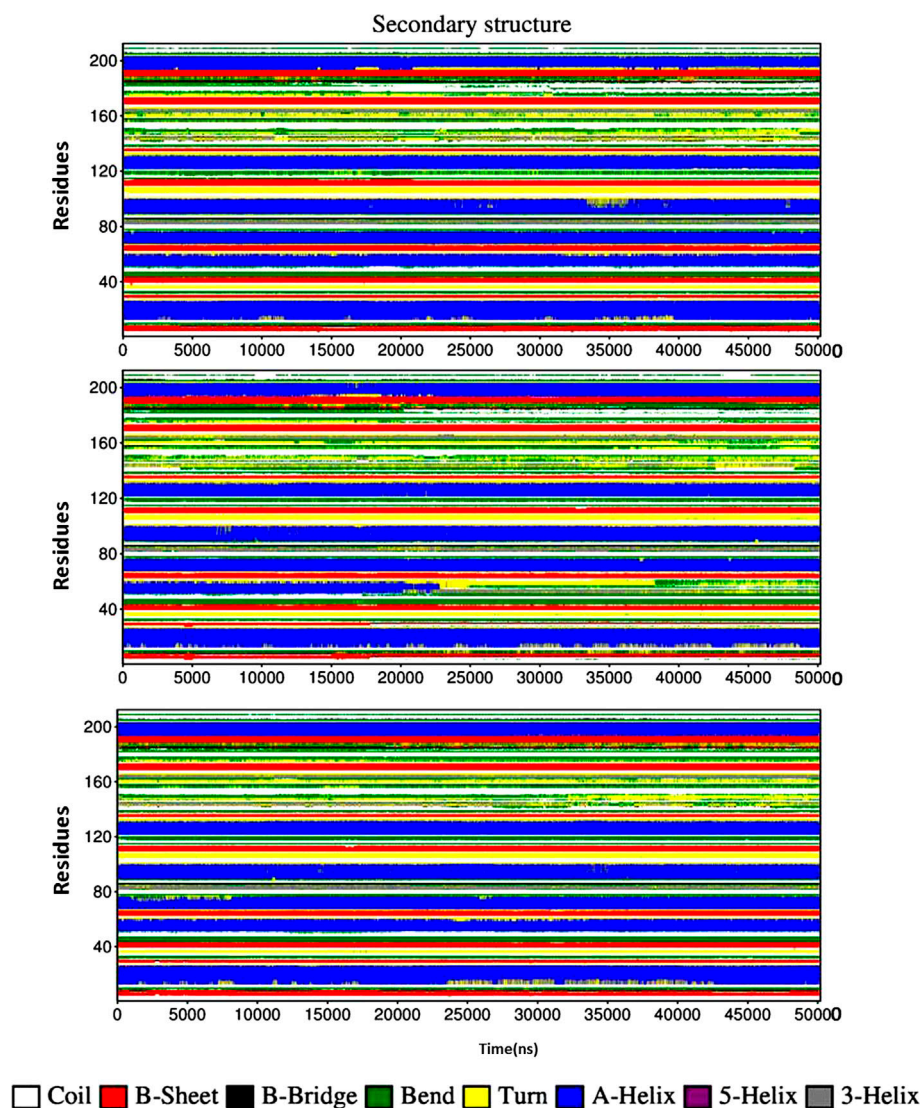


Figure 7. DSSP analysis of BARD1 BRCT (568-777) *wild-type*, Arg658Cys, and Ile738Val proteins with respect to time. Notes: (A) BARD1 BRCT (568-777) *wild-type*, (B) Ile738Val, and (C) Arg658Cys.

structure indicates that structure has lost rigidity (Figure 5(D)). BARD1 BRCT (568-777) *wild-type* and Arg658Cys mutant protein structures do not show any drastic change in the SASA values, in sharp contrast to Ile738Val mutant protein, which shows increase in the solvent accessible surface area during the initial phase of the simulation (Figure 5(E)). We have also observed significant differences in the hydrogen bonding pattern during the simulation. BARD1 BRCT (568-777) *wild-type* protein has shown better retention in hydrogen bonds over the period of stimulation compared to Ile738Val and Arg658Cys mutant protein structures (Figure 5(C)). Hydrogen bond sampling at every 10 ns further indicated that *wild-type* protein shows higher retention of hydrogen bond than the mutant proteins (Supplementary Figure 3). Loss of hydrogen bond formation leads to more flexible

conformation, and might result in loss of function of the mutant protein.

To understand the overall dynamics and evaluate the degree of flexibility, we have performed PCA and plotted eigenvector 1 v/s eigenvector 2 (Figure 6(B)–(D)). The area spanned/dispersion by this plot is indicative of the nature of motion. It has been observed that BARD1 BRCT (568-777) *wild-type* protein has the compact structure. Mutant Ile738Val is more flexible than BARD1 BRCT (568-777) *wild-type* and Arg658Cys proteins (Figure 6(A)). The DSSP plug-in of GROMACS monitored the secondary structures at different times during simulation (Kabsch & Sander, 1983). BARD1 BRCT Ile738Val mutant started losing the α -helix occurring between 50th and 60th residues and lost completely at about 25 ns (Figure 7(A) and (B)). However, no drastic

change in the secondary structure of *wild-type* and Arg658Cys mutant were observed (Figure 7(C)). It can be concluded that loss in α helical content in Ile738Val mutant protein may lead to structural flexibility. This was further supported by the change in volume recorded in DLS and fluorescence spectroscopic studies (Figure 5(F)).

3.5. Weak intramolecular interactions

Minimum energy structures of BARD1 BRCT (568-777) *wild-type*, Arg658Cys, and Ile738Val mutant proteins were used to study the weak intramolecular interactions. In the *wild-type* structure, Arg 658 forms hydrogen bond with the Glu 652, 649, and 655, and non-covalent interactions with Ser 660, Gly 656, Leu 662, and Arg 661. In Cys 658 mutant structure, there is a reduction in the number of hydrogen bonds. Furthermore, Cys 658 forms non-covalent interactions with Gly 656, Glu 652, Pro 654, Ile 653, and Ser 660 (Supplementary Figure 2 (A) and (B)). Mutant Ile738Val is involved in the hydrogen bonding with the Tyr 678 and non-hydrogen bonding interaction with Tyr 736, Phe 736, and Ala 758. Furthermore, Val 738 forms hydrogen bonds with Tyr 678 and a new hydrogen bond is established with Trp680 and non-hydrogen bonding interactions with Phe 683, Leu 679, Phe 677, Ala 758, and Tyr 736. Mutant structure Arg658Cys comprehensively loses the hydrogen bonds as compared to *wild-type* structure, further destabilizing the structure and surface charge of the protein molecule (Supplementary Figure 2 (C) and (D)).

4. Conclusions

To explore the structural effect of Arg658Cys and Ile738Val mutations on BARD1 BRCT, we have carried out biophysical experiments and MD simulations. In the crystal structure of BARD1 BRCT, Arg658 is a surface exposed residue, whereas Ile 738 is buried inside the structure. Expression and purification profile of BARD1 BRCT *wild-type* and mutant proteins do not show any drastic change in solubility and monomeric behavior. Secondary structures characterized by CD spectroscopy suggest that mutation is not inducing immense global changes, as the change in the ellipticity values is almost identical for all proteins. Far-UV spectra of proteins show insignificant change in the secondary structure, but slight local changes in the structure are also irrefutable. Near-UV CD spectroscopy, fluorescence spectroscopy, and limited proteolysis experiments suggested that the mutations are not affecting the overall compactness. The T_m value has reduced by 7 and 6.2°C for the mutants. Interestingly, the same concentration of GuHCl appears to be required to denature the *wild-type* and mutant proteins. Results from molecular dynamics simulation

indicated that Ile738Val structure has gain flexibility compared to *wild-type* and Arg658Cys mutant proteins. The gain of flexibility has been detected in RMSD, RMSF, and R_g plot for Ile738Val mutant, which is further supported by red shift in native fluorescence maximum, decrease in the number of hydrogen bonds, increase in volume, SASA, and PCA. Loss of T_m and ΔG of BARD1 BRCT and Arg658Cys and Ile738Val mutants with respect to *wild-type* suggests that substitutions are physiologically detrimental. It has been observed collectively that *wild-type* and mutant proteins exhibited analogous secondary structural constituents, whereas fluorescence spectroscopy suggested that the comparative positioning of Trp and Tyr were significantly hindered. MDS of BARD1 BRCT (568-777) *wild-type*, Arg658Cys, and Ile738Val mutant protein structures has been comprehensively analyzed to understand the structural alterations. Our results from the biophysical, *in vitro*, and *in silico* approaches predict that Arg658Cys and Ile738Val mutants are destabilizing the BARD1 BRCT domain which may lead to the loss of thermodynamic stability and functional activity.

Supplementary material

The supplementary material for this paper is available online at <http://dx.doi.org/10.1080/07391102.2015.1082149>.

Acknowledgments

The authors would like to acknowledge Mass Spectrometry, BTIS facility of TMC-ACTREC. MVH thanks DAE for the award of Raja Ramanna fellowship.

Disclosure statement

No potential conflict of interest was reported by the authors.

Funding

This work was supported by the Department of Biotechnology, Ministry of Science and Technology [grant number BT/PR10765/BRB/664/2008], [grant number BT/PR12565/BID/07/303/2009], [grant number DBT BT/513/NE/TBP/2013]; Seed in Air grant from TMC.

References

- Ahmed, M., & Rahman, N. (2006). ATM and breast cancer susceptibility. *Oncogene*, 25, 5906–5911.
- Alshatwi, A. A., Hasan, T. N., Syed, N. A., Shafi, G., & Grace, B. L. (2012). Identification of functional SNPs in BARD1 gene and *in silico* analysis of damaging SNPs: Based on data procured from dbSNP database. *PLoS One*, 7, e43939.
- Amadei, A., Linssen, A. B., & Berendsen, H. J. (1993). Essential dynamics of proteins. *Proteins: Structure, Function, and Genetics*, 17, 412–425.

- Antoniou, A. C., Beesley, J., McGuffog, L., Sinilnikova, O. M., Healey, S., Neuhausen, S. L., ... Easton, D. F. (2010). Common breast cancer susceptibility alleles and the risk of breast cancer for BRCA1 and BRCA2 mutation carriers: Implications for risk prediction. *Cancer Research*, 70, 9742–9754.
- Birrane, G., Varma, A. K., Soni, A., & Ladas, J. A. (2007). Crystal structure of the BARD1 BRCT domains. *Biochemistry*, 46, 7706–7712.
- Bork, P., Hofmann, K., Bucher, P., Neuwald, A. F., Altschul, S. F., & Koonin, E. V. (1997). A superfamily of conserved domains in DNA damage-responsive cell cycle checkpoint proteins. *FASEB Journal*, 11, 68–76.
- Brzovic, P. S., Meza, J. E., King, M. C., & Klevit, R. E. (2001). BRCA1 RING domain cancer-predisposing mutations: Structural consequences and effects on protein-protein interactions. *Journal of Biological Chemistry*, 276, 41399–41406.
- Brzovic, P. S., Rajagopal, P., Hoyt, D. W., King, M. C., & Klevit, R. E. (2001). Structure of a BRCA1-BARD1 heterodimeric RING-RING complex. *Nature Structural Biology*, 8, 833–837.
- Callebaut, I., & Mornon, J. P. (1997). From BRCA1 to RAP1: A widespread BRCT module closely associated with DNA repair. *FEBS Letters*, 400, 25–30.
- Collins, N., McManus, R., Wooster, R., Mangion, J., Seal, S., Lakhani, S. R., ... Easton, D. F. (1995). Consistent loss of the wild type allele in breast cancers from a family linked to the BRCA2 gene on chromosome 13q12-13. *Oncogene*, 10, 1673–1675.
- De Brakeleer, S., De Grève, J., Loris, R., Janin, N., Lissens, W., Sermijn, E., & Teugels, E. (2010). Cancer predisposing missense and protein truncating BARD1 mutations in non-BRCA1 or BRCA2 breast cancer families. *Human Mutation*, 31, E1175–E1185.
- Ghimanti, C., Sensi, E., Presciuttini, S., Brunetti, I. M., Conte, P., Bevilacqua, G., & Caligo, M. A. (2002). Germline mutations of the BRCA1-associated ring domain (BARD1) gene in breast and breast/ovarian families negative for BRCA1 and BRCA2 alterations. *Genes, Chromosomes & Cancer*, 33, 235–242.
- Harpaz, Y., Gerstein, M., & Chothia, C. (1994). Volume changes on protein folding. *Structure*, 2, 641–649.
- Heikkinen, K., Rapakko, K., Karppinen, S. M., Erkko, H., Knuutila, S., Lundan, T., ... Winqvist, R. (2006). RAD50 and NBS1 are breast cancer susceptibility genes associated with genomic instability. *Carcinogenesis*, 27, 1593–1599.
- Hess, B., Kutzner, C., van der Spoel, D., & Lindahl, E. (2008). GROMACS 4: Algorithms for highly efficient, load-balanced, and scalable molecular simulation. *Journal of Chemical Theory and Computation*, 4, 435–447.
- Jin, Y., Xu, X. L., Yang, M. C., Wei, F., Ayi, T. C., Bowcock, A. M., & Baer, R. (1997). Cell cycle-dependent colocalization of BARD1 and BRCA1 proteins in discrete nuclear domains. *Proceedings of the National Academy of Sciences*, 94, 12075–12080.
- Kabsch, W., & Sander, C. (1983). Dictionary of protein secondary structure: Pattern recognition of hydrogen-bonded and geometrical features. *Biopolymers*, 22, 2577–2637.
- Kaminski, G. A., Friesner, R. A., Tirado-Rives, J., & Jorgensen, W. L. (2001). Evaluation and reparametrization of the OPLS-AA force field for proteins via comparison with accurate quantum chemical calculations on peptides. *The Journal of Physical Chemistry B*, 105, 6474–6487.
- Kaplan, W., & Littlejohn, T. G. (2001). Swiss-PDB Viewer (Deep View). *Briefings in Bioinformatics*, 2, 195–197.
- Karppinen, S. M., Barkardottir, R. B., Backenhorn, K., Sydenham, T., Syrjakoski, K., Schleutker, J., ... Winqvist, R. (2006). Nordic collaborative study of the BARD1 Cys557Ser allele in 3956 patients with cancer: enrichment in familial BRCA1/BRCA2 mutation-negative breast cancer but not in other malignancies. *Journal of Medical Genetics*, 43, 856–862.
- Karppinen, S.-M., Heikkinen, K., Rapakko, K., & Winqvist, R. (2004). Mutation screening of the BARD1 gene: Evidence for involvement of the Cys557Ser allele in hereditary susceptibility to breast cancer. *Journal of Medical Genetics*, 41, 856–862.
- Kolchanov, N. A., Soloviov, V. V., & Zharkikh, A. A. (1983). The effects of mutations, deletions and insertions of single amino acids on the three-dimensional structure of globins. *FEBS Letters*, 161, 65–70.
- Li, M., & Yu, X. (2013). Function of BRCA1 in the DNA damage response is mediated by ADP-ribosylation. *Cancer Cell*, 23, 693–704.
- Meijers-Heijboer, H., van den Ouweland, A., Klijn, J., Wasielewski, M., de Snoo, A., Oldenburg, R., ... Stratton, M. R. (2002). Low-penetrance susceptibility to breast cancer due to CHEK2*1100delC in noncarriers of BRCA1 or BRCA2 mutations. *Nature Genetics*, 31, 55–59.
- Miki, Y., Swensen, J., Shattuck-Eidens, D., Futreal, P. A., Harshman, K., Tavtigian, S., ... Skolnick, M. H. (1994). A strong candidate for the breast and ovarian cancer susceptibility gene BRCA1. *Science*, 266, 66–71.
- Mohammad, D. H., & Yaffe, M. B. (2009). 14-3-3 proteins, FHA domains and BRCT domains in the DNA damage response. *DNA Repair*, 8, 1009–1017.
- Pace, C. N. (1986). Determination and analysis of urea and guanidine hydrochloride denaturation curves. *Methods in Enzymology*, 131, 266–280.
- Pace, C. N., & Shaw, K. L. (2000). Linear extrapolation method of analyzing solvent denaturation curves. *Proteins: Structure, Function, and Genetics*, 41, 1–7.
- Rapakko, K., Heikkinen, K., Karppinen, S. M., Erkko, H., & Winqvist, R. (2007). Germline alterations in the 53BP1 gene in breast and ovarian cancer families. *Cancer Letters*, 245, 337–340.
- Renwick, A., Thompson, D., Seal, S., Kelly, P., Chagtai, T., Ahmed, M., ... Rahman, N. (2006). ATM mutations that cause ataxia-telangiectasia are breast cancer susceptibility alleles. *Nature Genetics*, 38, 873–875.
- Ryckaert, J.-P., Ciccotti, G., & Berendsen, H. J. (1977). Numerical integration of the cartesian equations of motion of a system with constraints: molecular dynamics of n-alkanes. *Journal of Computational Physics*, 23, 327–341.
- Scully, R., Chen, J., Ochs, R. L., Keegan, K., Hoekstra, M., Feunteun, J., & Livingston, D. M. (1997). Dynamic changes of BRCA1 subnuclear location and phosphorylation state are initiated by DNA damage. *Cell*, 90, 425–435.
- Thai, T. H., Du, F., Tsan, J. T., Jin, Y., Phung, A., Spillman, M. A., ... Bowcock, A. M. (1998). Mutations in the BRCA1-associated RING domain (BARD1) gene in primary breast, ovarian and uterine cancers. *Human Molecular Genetics*, 7, 195–202.
- Thanassoulas, A., Nomikos, M., Theodoridou, M., Yannoukakos, D., Mastellos, D., & Nounesis, G. (2010). Thermodynamic study of the BRCT domain of BARD1 and its interaction with the -pSER-X-X-Phe- motif-containing BRIP1 peptide. *Biochimica et Biophysica Acta (BBA) – Proteins and Proteomics*, 1804, 1908–1916.

- Vikrant, Kumar, R., Yadav, L. R., Nakhwa, P., Waghmare, S. K., Goyal, P., & Varma, K. (2013). Structural and functional implication of RAP80 ΔGlu81 mutation. *PLoS One*, 8, e72707.
- Vikrant, Nakhwa, P., Badgujar, D. C., Kumar, R., Rathore, K. K. S., & Varma A. K. (2014). Structural and functional characterization of the MERIT40 to understand its role in DNA repair. *Journal of Biomolecular Structure and Dynamics*, 32, 2017–2032.
- Wooster, R., Neuhausen, S. L., Mangion, J., Quirk, Y., Ford, D., Collins, N., ... Averill, D. (1994). Localization of a breast cancer susceptibility gene, BRCA2, to chromosome 13q12-13. *Science*, 265, 2088–2090.
- Wu, L. C., Wang, Z. W., Tsan, J. T., Spillman, M. A., Phung, A., Xu, X. L., ... Baer, R. (1996). Identification of a RING protein that can interact *in vivo* with the BRCA1 gene product. *Nature Genetics*, 14, 430–440.
- Wu-Baer, F., Lagazon, K., Yuan, W., & Baer, R. (2003). The BRCA1/BARD1 heterodimer assembles polyubiquitin chains through an unconventional Linkage involving lysine residue K6 of ubiquitin. *Journal of Biological Chemistry*, 278, 34743–34746.
- Yoshikawa, K., Ogawa, T., Baer, R., Hemmi, H., Honda, K., Yamauchi, A., ... Takahashi, R. (2000). Abnormal expression of BRCA1 and BRCA1-interactive DNA-repair proteins in breast carcinomas. *International Journal of Cancer*, 88, 28–36.
- Zhukov, I., Jaroszewski, L., & Bierzynski, A. (2000). Conservative mutation Met8 → Leu affects the folding process and structural stability of squash trypsin inhibitor CMTI-I. *Protein Science*, 9, 273–279.